ESOMAT 2009, 02022 (2009)
DOI:10.1051/esomat/200902022

On the influence of crystal defects on the functional stability of NiTi based shape memory alloys

Burkhard Maass[a], Juri Burow, Jan Frenzel and Gunther Eggeler

Institute of Materials, Ruhr University Bochum, 44801 Bochum, Germany

Abstract. The cyclic application of the shape memory effect in NiTi based shape memory alloys is associated with a degradation of the functional properties. In the present work, we show how the functional stability of NiTi based shape memory alloys depends on various microstructural defects like grain boundaries, dislocations and substitutional elements (Fe replacing Ni). As a general trend, it was observed that thermal cycling results in a decrease in phase transformation temperatures. Nano-grained microstructures provide a significantly higher functional stability than coarse grained microstructures due to reduced dislocation activity. Cold work impedes phase transformation processes and provides a slight improvement of the functional stability. Fe additions to NiTi are associated with the occurance of two-step transformations (cooling: B2 ⇒ R ⇒ B19', heating: B19' ⇒ R ⇒ B2) which allow partial thermal cycling (B2 ⇔ R and R ⇔ B19'). We show that B2 ⇔ R cycling has a better stability than R ⇔ B19' cycling due to a better crystallographic compatibility between B2 and R.

1 Introduction

NiTi based shape memory alloys (SMAs) are interesting materials due to their good mechanical and functional properties, good biocompatibility, corrosion resistance and high specific electric resistance [1]. Most importantly, the shape memory effects (one-way effect, two-way effect, pseudoelasticity) in NiTi can be exploited many times. Today, NiTi SMAs are used in a wide technological range with focus on medical, actuator and special engineering applications [2–5]. The cyclic application of the shape memory effect is associated with a degradation of the functional properties. This process is often referred to as functional fatigue. One can observe cyclic changes in functional properties during thermal cycling using thermal analysis. It has been shown [6, 7] that thermal cycling of NiTi SMAs is associated with an increase in dislocation density during each cycle. These dislocations can impede elementary transformation processes which account for a decrease in transformation temperatures. Recently, we have published an article on thermo-mechanical cycling of NiTi based spring actuators where we show that the gradual increase in microstructural defects is associated with a limited crystallographic compatibility between the high and the low temperature phase [8]. Dislocations which are introduced during cycling help to accommodate transformation strains.

In the present work, we investigate functional fatigue of NiTi and NiTiFe SMAs by thermal cycling using differential scanning calorimetry (DSC). Since all types of microstructural defects have an influence on the martensitic transformation, we exemplarily concentrate on the effects of grain boundaries, dislocations resulting from cold work and alloy modifications (Fe atoms substituting Ni) on functional stability.

[a] e-mail: burkhard.maass@rub.de

Article available at http://www.esomat.org or http://dx.doi.org/10.1051/esomat/200902022

2 Experiments

2.1 Alloy production and sample preparation

In the present study, four different NiTi based SMAs were investigated by thermal cycling. The first material was a homogenized cast NiTi with 50 at.% Ni and a grain size of several millimeters. The second and third material differ from the first in terms of grain size and dislocation density. As a fourth material, we used a $Ni_{47}Ti_{50}Fe_3$ SMA. The alloys were prepared by melting Ni pellets (Ni: >99.98 wt.%) of an average size of 9 mm, Ti plates (Ti: >99.9 wt.%), 20x20x5 mm^3, and Fe shreds (Fe: >99.9 wt.%) of an average size of 5 mm. The Ti plates were ground with SiC emery paper (mesh-size 80) in order to remove oxide layers and cleaned using acetone and alcohol in an ultrasonic bath. Melting was performed using a Vacuum Arc Melter of type Edmund Buehler GmbH AM. The raw materials were placed in a water-cooled Cu-crucible. Prior to melting, the furnace was evacuated to $3 \cdot 10^{-5}$ mbar and then filled with Ar (> 99.999 vol.%) up to a pressure of 700 mbar. This process was repeated three times. After melting, the alloys were held in the liquid state for 20 s. In order to obtain a good ingot homogeneity, all ingots were turned over and remolten 5 times. Afterwards, the resulting ingots were welded into evacuated quartz-tubes and homogenized in a furnace of type Linn High Term LM312 for 24 h at 950°C.
To obtain a nano-grained (NG) wire, we used wire drawing which allowed a partial amorphization of the microstructure. In the final drawing step, the material was subjected to 60% cold work and crystallized/recrystallized at 400°C for 12 minutes, followed by water quenching. Further details on the wire drawing procedure are given elsewhere [9]. In order to investigate the influence of dislocations on the functional stability, a mild cold work (10% deformation) was applied using a rolling mill of type Buehler EW 200 x 120 A.

2.2 Thermal and microstructural analysis

The alloys were subjected to thermal cycling using a DSC device of type Netzsch DSC 204 F1 Phoenix. The heating/cooling rate was 10 °C/min. Fig. 1 gives an example of a typical DSC curve of a single cycle with a one-step transformation. All characteristic phase transformation temperatures are indicated (T_S, T_P, T_F). The start and finish temperatures were determined using the tangent method. Samples for DSC testing were prepared by grinding with SiC emery paper (mesh-size 320) and alcohol cleaning as described above. In the case of the nano-grained wire, a sample was cut off and ground in order to ensure good thermal contact with the DSC pan.

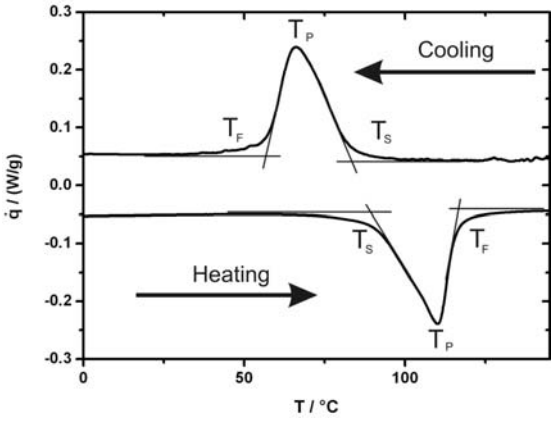

Fig. 1. Determination of start-, peak- and finish-temperatures

Transmission electron microscopy (TEM) was performed using a Philips CM20 analytical microscope operating at 200kV. Grain boundaries were studied in the high temperature phase heating the specimen to a nominal temperature of 200°C using a single tilt heating holder of type Philips PW 6592/00. Details on TEM sample preparation have been described elsewhere [10].

3 Results and discussion

Fig. 2 shows a compilation of 20 DSC cycles of a binary NiTi alloy. This material has low densities of grain boundaries, dislocations and substitutional atoms. We use this material state as a reference and show how the functional behavior changes once we apply thermomechanical treatments or add Fe (replacing Ni). The material shows one-step transformations on cooling and heating. The peaks are associated with the transformation B2 ⇒ B19' on cooling and B19' ⇒ B2 on heating. It can be seen that thermal cycling is associated with a shift of all characteristic transformation temperatures to lower values. The effect has the highest intensity in the early cycles, while it continiously decays and eventually reaches a saturation value with increasing cycle numbers. Most importantly, 20 thermal cycles result in a shift of the martensite start temperature of about 21.2°C on cooling. Tab. 1 shows the shifts of all characteristic transformation temperatures after 20 thermal cycles.

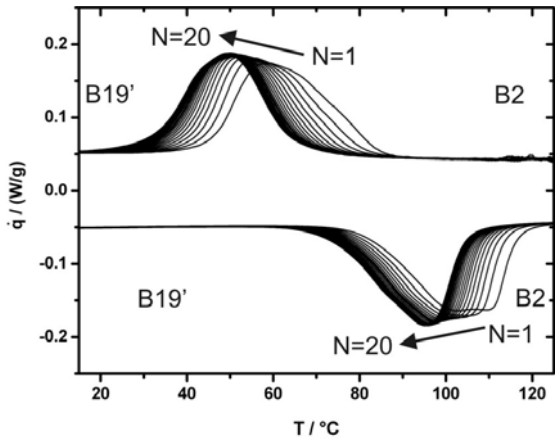

Fig. 2. Compilation of 20 DSC-cycles of the reference material

Table 1. Transformation temperature shifts after 20 thermal cycles for binary NiTi with different microstructures

	$\Delta\ \mathbf{T}_S$ / °C	$\Delta\ \mathbf{T}_P$ / °C	$\Delta\ \mathbf{T}_F$ / °C
NiTi, homogenized			
B2 ⇒ B19'	21.2	9.6	13.3
B19' ⇒ B2	8.1	7.4	11.9
NiTi, cold worked			
B2 ⇒ B19'	13.7	2	4.8
B19' ⇒ B2	5.6	7.9	19
NiTi, NG			
B2 ⇒ R	0.4	0.1	0.2
R ⇒ B19'	1.7	2.7	0.6
B19' ⇒ B2	0.1	0.3	0.5

Fig. 3 shows a TEM micrograph of a NiTi SMA wire with nano-grains. It can be seen that the grain size of the high temperature phase is lower than 100nm. Internal interfaces have a strong effect on the martensitic transformation, e.g. [9,11], and on the functional stability. Fig. 4 shows 20 DSC cycles of our NG wire. In contrast to our reference material (Fig. 2), a two-step transformation on cooling can be observed. The two DSC peaks are associated with the B2 ⇒ R and the R ⇒ B19' transformations. The single peak on heating is associated with a direct B19' ⇒ B2 reverse transformation. This transformation behavior represents a typical feature of ultra-fine grained NiTi [11]. Generally, the transformation B2 ⇒ B19' which was observed in the coarse grained reference material (Fig. 2) is associated with a relatively large transformation strain [12] related to the corresponding lattice shear process. Coarse grained microstructures only have a few grain boundaries which act as obstacles for elementary lattice shear processes. In contrast, a high density of internal interfaces in NG SMAs makes the martensitic transformation B2 ⇒ B19' more difficult because twinning accomodation is impeded by B2 grain boundaries imposing geometrical constraints. The B2 ⇒ R transformation with its significantly smaller transformation strain [11,12] requires less accomodation and thus is less affected by grain boundaries. And this seems to be the reason for the changes in transformation character from one to two-step as the grain sizes strongly decrease.
Fig. 4 shows that the R ⇒ B19' transformation occurs over a wide temperature range with low local intensities. It seems reasonable to assume that this also reflects the obstacle character of internal interfaces. In case of our coarse grained reference material, a few martensite nucleation events in combination with a high transformation front mobility promote a direct one-step transformation, indicated by a narrow DSC peak, (Fig. 2). In case of the nano-structured material, it is difficult for the transformation front to overcome grain boundaries. Nucleation needs to occur in each nano-grain. The nano-grained microstructure approaches thermodynamic equilibrium by first transforming into R-phase. Stronger undercooling associated with higher driving forces eventually results in the formation of B19' martensite, nano-grain by nano-grain.

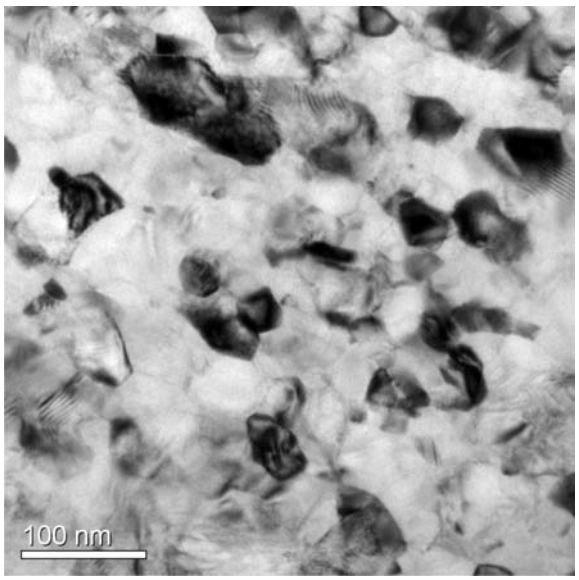

Fig. 3. Microstructure of the NG wire

One striking result is that the nano-grained wire has an outstanding functional stability, Fig. 4. All 20 DSC curves in Fig. 4 almost perfectly coincide. In contrast to the coarse grained reference material, no significant shift in transformation temperatures is associated with thermal cycling, Tab. 1. The reason for the high functional stability of NG SM wires is that the high density of internal interfaces strongly reduces dislocation activity.

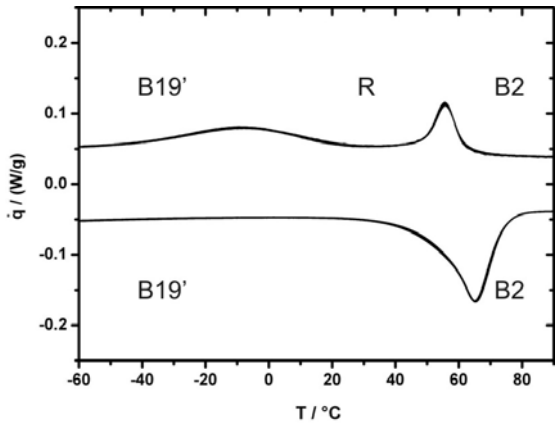

Fig. 4. Compilation of 20 DSC-cycles of the NG wire

Now, we come to the effect of dislocations resulting from mild cold work on the functional stability. Fig. 5 shows a compilation of 20 DSC cycles of binary NiTi which was subjected to 10 % cold work by rolling. The DSC peaks are broad and the transformation heats (corresponding to the area below each peak) are smaller than in the case of the reference material, Fig. 2. This suggests that higher densities of processing dislocations hamper phase transformation processes on cooling and heating as previously reported [13]. It is difficult to provide a clear conclusion on whether the functional stability of cold rolled NiTi is better than in the case of the reference material. While the shifts in transformation temperatures on cooling are smaller than in the case of the refence material, the opposite holds for the peak and finish temperatures of the reverse transformation, Tab. 1. The peak associated with the transformation B19'⇒ B2 on heating initially appears as relatively flat. During cycling, it becomes more and more pronounced, Fig. 5. We assume that the dislocation structure changes during thermal cycling. Further work is required to clarify the interplay between dislocation plasticity and phase transformation processes in NiTi.

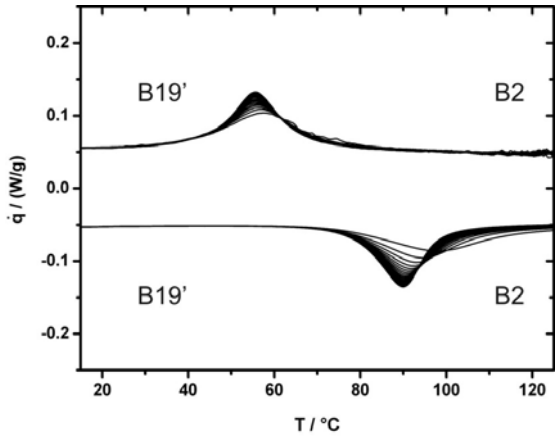

Fig. 5. Compilation of 20 DSC-cycles of $Ni_{50}Ti_{50}$, subjected to 10% cold work

The addition of Fe atoms to binary NiTi replacing Ni results in a significant change in phase transformation behavior. Fig. 6 shows a compilation of 20 DSC cycles for the NiTiFe alloy. This material shows a two-step transformation on both, cooling and heating. The DSC peaks are associated with the transformations B2 ⇒ R and R ⇒ B19' on cooling and B19' ⇒ R and R ⇒ B2 on heating [12]. Fig. 6 shows that thermal cycling is associated with a decrease in maximum heat flow for the B2 ⇒ R peak and a shift of the R ⇒ B19' peak by approx. 30°C to lower temperatures. Similar observations were made for the DSC peaks associated with the reverse transformation on heating, although the temperature shift is less intense, Tab. 2.

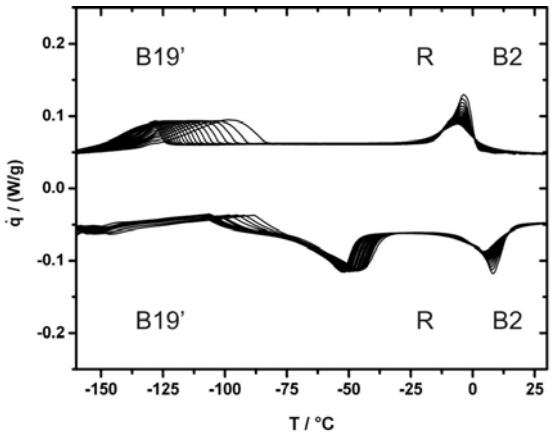

Fig. 6. Compilation of 20 DSC-cycles of $Ni_{47}Ti_{50}Fe_3$

Table 2. Transformation temperature shifts after 20 thermal cycles of the NiTiFe alloy

	$\Delta\ \mathbf{T}_S$ / °C	$\Delta\ \mathbf{T}_P$ / °C	$\Delta\ \mathbf{T}_F$ / °C
$Ni_{47}Ti_{50}Fe_3$			
Complete cycling			
B2 ⇒ R	3.6	2.9	9.1
R ⇒ B2	9.4	3.9	2.1
R ⇒ B19'	41.1	31.7	20.2
B19' ⇒ R	2.1	6.7	10.5
Separated cycling			
B2 ⇒ R	0.1	0.1	0.0
R ⇒ B2	0.0	0.0	0.0
R ⇒ B19'	34	30.8	23.1
B19' ⇒ R	0.4	13.7	15.3

In order to clarify the role of the different types of martensitic transformations in NiTiFe alloys on defect accummulation during thermal cycling, we performed additional thermal cycling experiments where the maximum and minimum testing temperatures were chosen such, that only one type of transformation and the associated reverse transformation occurred. The materials were exclusively subjected to B2 ⇔ R and R ⇔ B19' transformations, respectively. We refer to this type of experiment as partial thermal cycling. Fig. 7 shows DSC charts from thermal cycling experiments where the transformations of type B2 ⇒ R (on cooling) and R ⇒ B2 (on heating) were considered. It can be seen that DSC curves of all 20 cycles almost perfectly coincide and that there are no significant changes of the transformation temperatures, Tab. 2. In contrast, the peaks associated with the transformations R ⇒ B19' and B19' ⇒ R significantly shift to lower temperatures during partial thermal cycling, Fig. 8. Our results indicate that this

type of transformation introduces a much larger amount of defects into the microstructure. We can explain these observations on the basis of a scenario where dislocations are introduced into the microstructure in each thermal cycle which help to accommodate transformation strains. The transformation of type B2 ⇒ R has a relatively low transformation strain [12,14] and thus requires less accommodation. In contrast, the transformation R ⇒ B19' has a significantly higher transformation strain and thus requires more accommodation. The latter is associated with the generation of larger amounts of dislocations since accommodation strains in NiTi are not only accommodated by twinning [6–8].

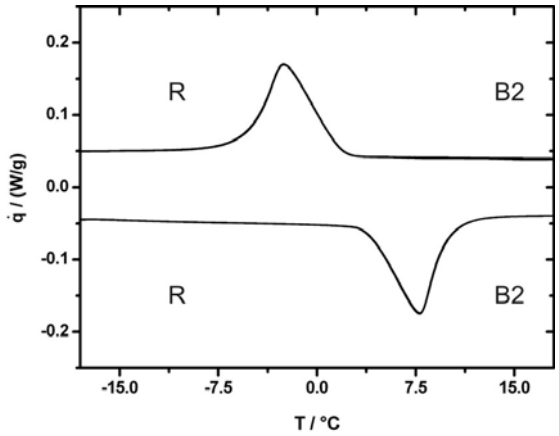

Fig. 7. Compilation of 20 DSC-cycles of $Ni_{47}Ti_{50}Fe_3$, transformation B2 ⇔ R

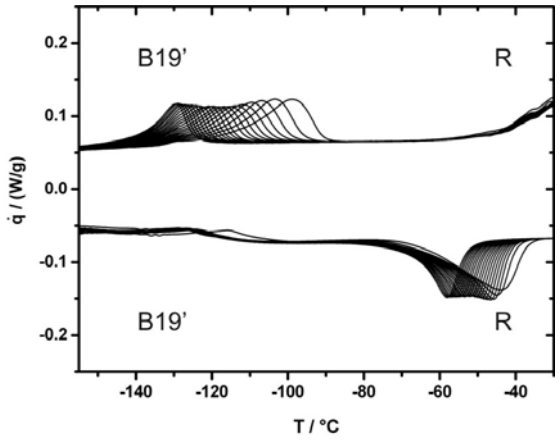

Fig. 8. Compilation of 20 DSC-cycles of $Ni_{47}Ti_{50}Fe_3$, transformation R ⇔ B19'

4 Summary and conclusion

In the present study, we investigate how the functional stability of NiTi based SMAs during thermal cycling is affected by various types of microstructural defects. As a reference material, an equiatomic, homogenized cast NiTi is used. The other materials are nano-structured NiTi, cold worked NiTi and a $Ni_{47}Ti_{50}Fe_3$ SMA. The following conclusions can be drawn:

1. Thermal cycling results in a shift of the phase transformation temperatures to lower values.
2. One possibility to improve functional stability is to establish nano structures of the high temperature phase. Internal interfaces reduce dislocation activity which accounts for changes in functional properties.
3. Cold work partially improves functional stability in NiTi. It was found that the DSC chart features associated with the martensitic transformation are more stable during cycling than in case of the reference material. The peak associated with the reverse transformation is shifted towards lower temperatures.
4. Fe atoms in NiTi promote two-step transformations (B2 $\Rightarrow$ R and R $\Rightarrow$ B19') on cooling and heating (B19' $\Rightarrow$ R and R $\Rightarrow$ B2). Cycling through the complete transformation range is associated with significant changes in transformation temperatures. Partial thermal cycling experiments show that these defects are mainly generated during the transformation R $\Leftrightarrow$ B19'. No changes in the transformation behavior result from the B2 $\Leftrightarrow$ R transformation. The B2 $\Leftrightarrow$ R transformation is associated with a lower transformation strain than R $\Leftrightarrow$ B19' transformations, which results in less microstructural changes during thermal cycling.

Acknowledgment

The authors acknowledge funding through project C7 of the collaborative research centre SFB459 (Shape Memory Technology) funded by the Deutsche Forschungsgemeinschaft (DFG), North Rhine-Westphalia and the Ruhr University Bochum and through the research group FOR 544 on ultra fine grained metallic materials coordinated by H.J. Maier (University of Paderborn), funded by the Deutsche Forschungsgemeinschaft (DFG).

References

1. H. Funakubo, *Shape Memory alloys* (Gordon and Breach, New York 1984)
2. T. Duerig, K.N. Melton, D.Stöckel, C.M. Wayman, *Engineering Aspects of Shape Memory Alloys* (Butterworth-Heinemann, London 1990) pp. 394-413
3. G. Eggeler, E. Hornbogen, A. Yawny, A. Heckmann, M. Wagner, Mat. Sci. and Eng. A **378**, (2004) pp.24-33
4. T. Duerig, A. Pelton, D. Stoeckel, Mat. Sci. and Eng. A **273-275**, (1999) pp.149-160
5. A. Schuster, H. Voggenreiter, M. Mertmann, Proc. Adaptronik-Congress Potsdam, (2000) pp.71-76
6. J. Perkins, Met. Trans. **4**, (1973) pp. 2709-2721
7. S. Miyazaki, Y. Igo, K. Otsuka, Acta Metall. **34**, (1986) p. 2045
8. Ch. Grossmann, J. Frenzel, V. Sampath, T. Depka, G. Eggeler, Met. Trans. A **in print**, (2009)
9. J. Burow, E. Prokofiev, Ch. Somsen, J.Frenzel, R. Valiev, G. Eggeler, Materials Science Forum **584-586**, (2008) pp. 852-857
10. J. Khalil-Allafi, A. Dlouhy, G. Eggeler, Acta Mater. **50**, (2002) p. 4255
11. T. Waitz, H.P. Karnthaler, Acta Mater. **52**, (2004) p. 5461
12. K. Otsuka, X. Ren, Prog. Mater. Sci. **50**, (2005) p. 511
13. Ch. Grossmann, J. Frenzel, V. Sampath, T. Depka, A. Oppenkowski, Ch. Somsen, K.Neuking, W. Theisen, G. Eggeler, Mat.-Wiss. u. Werkstofftechnik **39**, (2008) pp. 499-510
14. J. Khalil-Allafi, W.W. Schmahl, D.M. Toebbens, Acta Mater. **54**, (2006) p. 3171